SciEn

*Proceedings of 8th International Conference on Mechanical Engineering and Renewable Energy 2025*
*10-12 December, 2025, Chattogram, BANGLADESH*

SciEn Conference Series: Engineering Vol. 4, 2026, pp 73-77 https://doi.org/10.38032/scse.2026.4.42

# Lead-Free Fluoride Perovskite $AgCdF_3$ for High-Efficiency Solar Cells: A Simulation-Guided Study

*Utsa Bhowmik*, Omkar Chowdhury*

Department of Electrical and Electronic Engineering, CUET, Chattogram-4349, Bangladesh

**ABSTRACT**

Lead-free fluoride perovskites are proving to be promising absorbers for next-generation solar cells due to their superior stability and environmentally friendly composition. In this work, we investigate $AgCdF_3$ as an absorber for single-junction perovskite solar cells using SCAPS-1D simulations, building upon insights from density functional theory. The proposed device architecture, ITO/$ZrS_2$/$AgCdF_3$/NiO/Au, was systematically optimized by examining hole and electron transport layers (NiO and $ZrS_2$), absorber and transport layer thicknesses, bulk and interface defect densities, and operating temperature. $AgCdF_3$ exhibits an indirect bandgap of 1.106 eV, a stable cubic structure, and enhanced ductility, indicating excellent mechanical robustness. Optimization results reveal that NiO as HTL and $ZrS_2$ as ETL provide ideal band alignment, minimal interfacial recombination, and efficient charge extraction. The absorber thickness of ~700 nm maximized photon absorption while balancing recombination losses. Bulk defect densities must be maintained below $10^{15}$ $cm^{-3}$ to preserve high device performance, while interface defects significantly influence open circuit voltage and fill factor. Under optimized conditions, the simulated device achieved $V_{oc}$ = 0.9081 V, $J_{sc}$ = 41.316 mA/$cm^2$, FF = 87.28%, and a maximum power conversion efficiency of 32.75%, retaining 26.75% efficiency at 400 K, demonstrating remarkable thermal stability. These findings highlight $AgCdF_3$'s potential as a high-efficiency, thermally robust, and lead-free perovskite absorber, offering a viable pathway for environmentally sustainable and high-performance photovoltaic applications.

Keywords Fluoride perovskite ($AgCdF_3$), High-efficiency solar cell, SCAPS-1D simulation, HTL/ETL optimization

Copyright @ All authors

This work is licensed under a Creative Commons Attribution 4.0 International License.

## 1. Introduction

An increase in global energy consumption, paired with the adverse ecological consequences of fossil fuels, has made it increasingly imperative to develop renewable and sustainable energy sources [1-2]. Solar energy, in particular, offers a clean and abundant resource, and the development of stable and efficient solar cells is crucial for addressing the global crisis. Among various photovoltaic technologies, perovskite solar cells (PSCs) have shown an extraordinary improvement in power conversion efficiency (PCE), increasing from a mere 3.8 % to over 26 % within just a decade [3-5]. This rapid progress is largely due to the exceptional optoelectronic properties of halide perovskites, including tunable band gaps, high absorption coefficients, long charge diffusion lengths, low exciton binding energies, and high carrier mobility [6].

While organic–inorganic hybrid perovskites have achieved high PCEs, their inherent instability—particularly thermal instability below 150 °C—limits their practical application [7]. These challenges have motivated researchers to explore more thermally stable, lead-free perovskites, including fluoride-based compounds with the general formula $ABF_3$ (A and B are cations, F is a monovalent fluorine anion). Fluoride perovskites have shown unique characteristics such as temperature superconductivity, colossal magnetoresistance, photoluminescence, thermoelectricity, and optical activity [8].

In recent years, density functional theory (DFT) and first-principles calculations have provided deep insights into the structural, electronic, optical, and mechanical properties of fluoride perovskites. Studies on silver-based perovskites, such as $AgMF_3$ (M = Zn, Cd, Co, Ni) and $AgXCl_3$ (X = Ca, Sr), have demonstrated chemical stability, ductility, and suitable band gaps for photovoltaic and thermoelectric applications [9]. $AgCdF_3$ has recently drawn interest because of its unique electronic and structural properties, which extend beyond conventional halide perovskites. Initially investigated for its potential in thermoelectric applications, $AgCdF_3$ demonstrated a relatively high thermoelectric figure of merit (ZT), arising from its low lattice thermal conductivity and favorable carrier transport characteristics. These findings highlighted the material's intrinsic ability to maintain efficient charge transport while suppressing thermal losses, a combination equally desirable in photovoltaic devices [10]. Building on this foundation, researchers have begun exploring $AgCdF_3$ in optoelectronic contexts, where its suitable bandgap, high absorption coefficient, and inherent stability make it a strong contender for high-performance solar cell applications [11].

Despite these theoretical insights, limited work has been conducted on evaluating $AgCdF_3$ at the device level for photovoltaic applications. Understanding how each layer in a PSC—including the transparent conductive oxide (TCO), electron transport layer (ETL), hole transport layer (HTL),

*Corresponding Author Email Address: u1902128@student.cuet.ac.bd 

perovskite absorber layer (PAL), and back-metal contact—affects overall performance is crucial [12]. Moreover, optical absorption, carrier generation and recombination, and interfacial engineering all play decisive roles in determining open-circuit voltage ($V_{oc}$), short-circuit current density ($J_{sc}$), and fill factor (FF) [13-15].

Table 1: Input parameters of TCO, ETL, HTL, and absorber layer

| Parameter | ITO | $TiO_2$ | $WO_3$ | $Al_2O_3$ |
|---|---|---|---|---|
| Thickness (nm) | 500 | 20 | 20 | 10 |
| Bandgap, Eg(eV) | 3.5 | 3.2 | 3.91 | 6 |
| Electron affinity, χ(eV) | 4 | 4.1 | 4.31 | 4.3 |
| Dielectric permittivity, $\mu_r$ | 9 | 9 | 8.9 | 13 |
| CB effective density of states | 2.2e18 | 2.2e18 | 3.7e18 | 2.2e18 |
| VB effective density of states | 1.8e19 | 1e19 | 3.1e18 | 1.8e19 |
| e- mobility ($cm^2$/Vs) | 20 | 20 | 1.1 | 100 |
| h+ mobility($cm^2$/Vs) | 10 | 10 | 10 | 20 |
| Shallow uniform donor density | 1e21 | 1e18 | 1e20 | 1e19 |
| Shallow uniform acceptor density | 0 | 0 | 0 | 0 |
| Total defect density | 1e15 | 1e15 | 1e15 | 1e15 |
| Reference | [17] | [18] | [18] | [18] |

| $BaSnO_3$ | $SnS_2$ | $ZrS_2$ | $AgCdF_3$ | NiO |
|---|---|---|---|---|
| 60 | 100 | 20 | 700 | 50 |
| 3.16 | 1.85 | 2.5 | 1.106 | 3.8 |
| 3.8 | 4.26 | 4.1 | 4.27 | 1.46 |
| 17 | 17.7 | 16.4 | 2.81 | 10.7 |
| 1.2e19 | 7.32e18 | 2.2e18 | 1.107e17 | 2.8e19 |
| 1.8e19 | 1e19 | 1.8e19 | 2.3e17 | 1e19 |
| 200 | 1e7 | 2.3e3 | 831 | 12 |
| 25 | 50 | 1.3e3 | 54 | 2.8 |
| 1e18 | 9.85e18 | 1e15 | 0 | 0 |
| 0 | 0 | 0 | 8.36e7 | 1e18 |
| 1e15 | 1e15 | 1e15 | 1e15 | 1e15 |
| [18] | [18] | [18] | [18] | [19] |

In this study, we applied SCAPS-1D simulations to investigate $AgCdF_3$ as an absorber layer for single-junction PSCs. Three different device configurations are examined to evaluate the effects of absorber and transport layer thickness, interface defects, back-contact work function, and operating temperature on photovoltaic performance. This approach aims to bridge the gap between theoretical predictions and practical device optimization, highlighting $AgCdF_3$'s potential as a stable and high-efficiency lead-free perovskite absorber.

## 2. GOVERNING EQUATIONS

All simulations were performed using SCAPS-1D (Version 3.3.09), a one-dimensional solar cell simulator that numerically solves the Poisson equation and carrier continuity equations to model charge transport and recombination. The governing equations are presented below:

(1). *Poisson's equation* describes the relationship between electric potential (φ), charge density, and dielectric constant:

$$d^2\varphi/dx^2 = (q/\varepsilon)(n - p) \text{ ----------(1)}$$

(2). *Carrier continuity equations* represent the conservation of charge for electrons and holes:

$$\partial n/\partial t=(1/q)\partial J_n/\partial x+(G–R)\text{----------(2)}$$

$$\partial p/\partial t=(-1/q)\partial J_p/\partial x+(G_p–R_p)\text{--------(3)}$$

(3). *Drift-diffusion equations* define the current densities of electrons and holes:

$$J_n=qD_n(\partial n/\partial x)-q\mu_n n(\partial\varphi/\partial x)\text{----------(4)}$$

$$J_p=qD_p\,(\partial p/\partial x)-q\mu_p p(\partial\varphi/\partial x)\text{---------(5)}$$

Where $q$ is the elementary charge (C), $n$ and $p$ are the electron and hole concentrations ($cm^{-3}$), $\varepsilon$ is the dielectric constant, $\varphi$ is the electric potential (V), $R$ is the carrier recombination rate ($cm^{-3}s^{-1}$), $G$ is the carrier generation rate ($cm^{-3}s^{-1}$), $J_n$ and $J_p$ are the current densities of electrons and holes ($mA/cm^2$), $D_n$ and $D_p$ are the diffusion coefficients for electrons and holes ($cm^2/s$), and $\mu_n$ and $\mu_p$ represent the mobility of electrons and holes ($cm^2$/ (V.s)) [16].

## 3. Device Structure and Simulation Methodology

The $AgCdF_3$-based solar cell was modeled as a single-junction device with the architecture ITO/$ZrS_2$/$AgCdF_3$/NiO/Au (Fig. 1), where ITO is the transparent conductive oxide, $ZrS_2$ is the electron transport layer (ETL), $AgCdF_3$ is the perovskite absorber layer (PAL), NiO is the hole transport layer (HTL), and Au serves as the back contact.

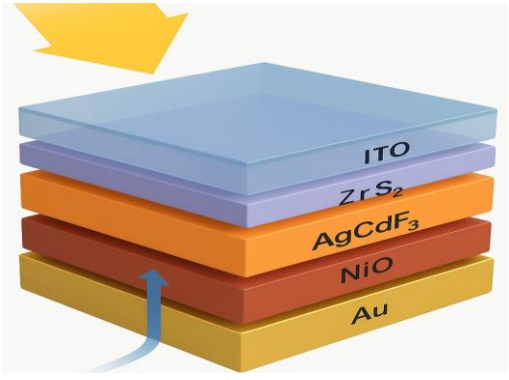


**Fig. 1:** Design of $AgCdF_3$-based perovskite solar cell

The energy band alignment is shown in Fig. 2.

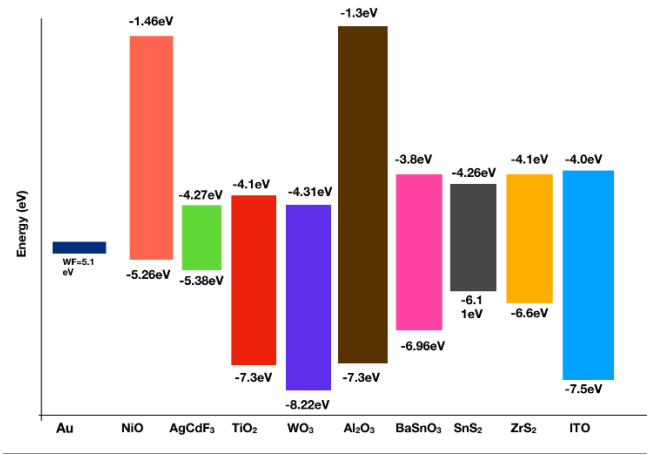


**Fig. 2:** Band energy alignment of corresponding layers

Simulations were performed using SCAPS-1D. Material parameters, layer thicknesses, and interface defect densities are listed in Tables 1 and 2.

**Table 2:** Interface defects employed in the simulated model.

| Parameters | ETL/Absorber | Absorber/HTL |
|---|---|---|
| Defect type | Neutral | Neutral |
| Capture cross-section $e^-$s ($cm^2$) | $10^{-15}$ | $10^{-18}$ |
| Capture cross-section $h^+$s ($cm^2$) | $10^{-15}$ | $10^{-16}$ |
| Energetic distribution | Single | Single |
| Reference for defect energy level ($E_t$) | Above the highest $E_v$ | Above the highest $E_v$ |
| Energy for reference (eV) | 0.6 | 0.05 |
| Total defect ($1/cm^2$) | $10^{15}$ | $10^{15}$ |

The effects of absorber and transport layer thickness, interface defects, and temperature on $V_{oc}$, $J_{sc}$, FF, and PCE were analyzed, and the JV characteristics of the optimized device are presented in Fig. 3

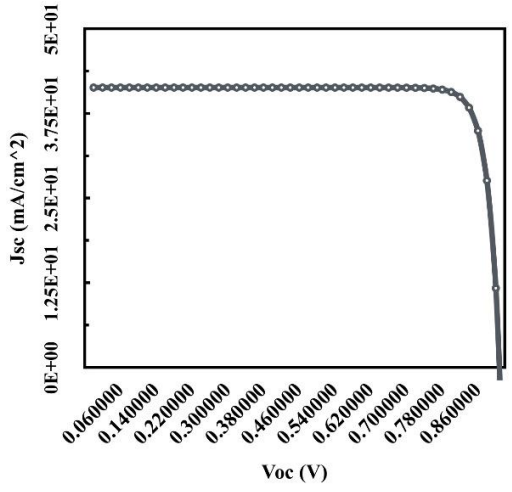


**Fig. 3:** J-V characteristic curve

## 4. Results and Discussion

The results are analyzed for material selection, thickness optimization, defect analysis, and thermal stability.

### 4.1 HTL SELECTION

In our efforts to enhance the PV performance of the $AgCdF_3$–based perovskite solar cell, we first reexamined the hole-transport layer (HTL), replacing CuI with NiO (Table 3). Despite CuI's notably high hole mobility, our simulations revealed that NiO offered superior valence-band alignment and lower interface recombination, ultimately boosting both open-circuit voltage ($V_{oc}$) and fill factor (FF). This enhancement stems from NiO's valence-band maximum lying closer to that of $AgCdF_3$, reducing the energetic barrier for hole extraction by approximately 0.07 eV. Additionally, NiO's higher dielectric constant affords greater screening of interfacial charge traps and broader depletion width, mitigating recombination pathways. These combined advantages outweighed CuI's mobility advantage in our thin-film architecture, leading to a modest but meaningful efficiency gain—from 27.12% with CuI to 28.05 % with NiO.

**Table 3:** Performance comparison between the reference device and the NiO-based modified device

| Optimized device configuration | $V_{oc}$ (V) | $J_{sc}$ ($mA/cm^2$) | FF (%) | PCE (%) |
|---|---|---|---|---|
| ITO/ZnO/$AgCdF_3$/CuI/Au | 0.823 | 42.472 | 77.62 | 27.12 |
| ITO/ZnO/$AgCdF_3$/NiO/Au | 0.830 | 42.21 | 80.04 | 28.05 |

### 4.2 ETL SELECTION

With the improved HTL in place, we proceeded to explore various electron-transport layers (ETLs), including $TiO_2$, $WO_3$, $Al_2O_3$, $BaSnO_3$, $SnS_2$, and $ZrS_2$, to identify an ideal counterpart for $AgCdF_3$. Among them, $ZrS_2$ emerged as the most promising candidate, achieving a simulated efficiency of 28.13 %. The superior performance derives primarily from $ZrS_2$'s exceptionally high electron mobility—several orders of magnitude greater than the other ETLs tested—significantly reducing the series resistance and thereby enhancing the fill factor.

**Table 4:** Optimized PV parameters of the AgCdF3-based solar cell for NiO HTL with Au back contact and different ETLs ($TiO_2$, $WO_3$, $Al_2O_3$, $BaSnO_3$, $SnS_2$, and $ZrS_2$)

| Optimized device configuration | $V_{oc}$ (V) | $J_{sc}$ ($mA/cm^2$) | FF (%) | PCE (%) |
|---|---|---|---|---|
| ITO/$TiO_2$/$AgCdF_3$/NiO/Au | 0.8370 | 41.82 | 80.30 | 28.11 |
| ITO/$WO_3$/$AgCdF_3$/NiO/Au | 0.8369 | 41.71 | 80.31 | 28.03 |
| ITO/$Al_2O_3$/$AgCdF_3$/NiO/Au | 0.8366 | 41.71 | 80.30 | 28.02 |
| ITO/$BaSnO_3$/$AgCdF_3$/NiO/Au | 0.8373 | 41.82 | 80.21 | 28.09 |
| ITO/$SnS_2$/$AgCdF_3$/NiO/Au | 0.8368 | 41.81 | 80.30 | 28.10 |
| ITO/$ZrS_2$/$AgCdF_3$/NiO/Au | 0.8374 | 41.82 | 80.32 | 28.13 |

### 4.3 THICKNESS ANALYSIS OF ABSORBER, HTL, AND ETL

The absorber thickness was varied from 200 nm to 1200 nm, revealing that $J_{sc}$ increased steadily (31.58 mA/cm² to 42.95 mA/cm²) due to enhanced photon absorption, whereas $V_{oc}$ decreased (0.898 V to 0.808 V) from increased bulk recombination. The FF slightly dropped (82.17% to 79.04%) owing to elevated series resistance, leading the PCE to rise from 23.30% to a peak of 28.13% at 700 nm before marginally declining, identifying ~700 nm as optimal (Fig. 4).

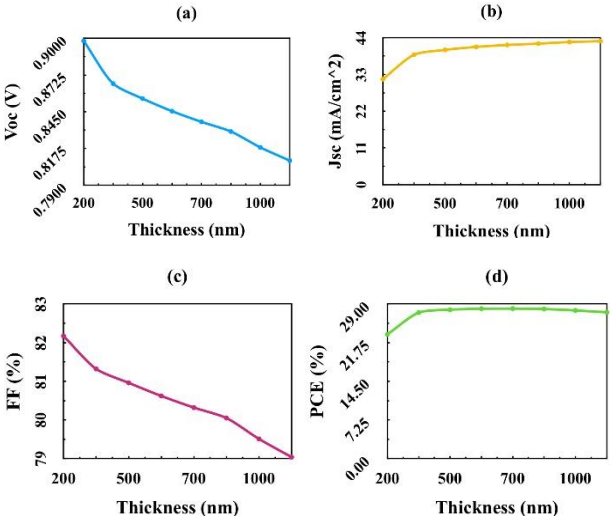


**Fig. 4:** $V_{oc}$(a), $J_{sc}$(b), FF(c), and efficiency(d) as a function of $AgCdF_3$-absorber layer thickness

Varying NiO (HTL) and $ZrS_2$ (ETL) thicknesses (20–200 nm) produced negligible changes in all PV parameters, confirming that within this range both layers enable efficient carrier extraction and transport without significant optical or resistive losses.

### 4.4 DEFECT DENSITY ANALYSIS OF THE $AgCdF_3$ ABSORBER

The bulk defect density ($N_t$) of the $AgCdF_3$ absorber was varied from $10^{12}$ to $10^{20}$ $cm^{-3}$ to assess its influence on photovoltaic performance. Increasing $N_t$ led to a pronounced decrease in $V_{oc}$ from 1.1859 V to 0.2377 V, driven by intensified Shockley–Read–Hall (SRH) recombination, which reduces the quasi-Fermi level separation. $J_{sc}$ remained nearly constant (41.82 mA/cm²) for $N_t$ values up to $10^{16}$ $cm^{-3}$ but dropped sharply to 2.73 mA/cm² at $10^{20}$ $cm^{-3}$ due to severe carrier lifetime reduction. The fill factor declined steadily from 82.67% to 35.61%, resulting in a substantial drop in PCE from 41.01% to 0.23%. These results highlight the necessity of maintaining $N_t$ below $10^{15}$ $cm^{-3}$ to ensure optimal device efficiency in $AgCdF_3$-based solar cells.

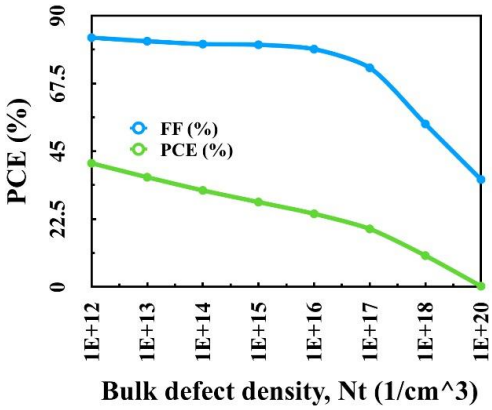


**Fig. 5:** FF and efficiency as a function of bulk defect density of $AgCdF_3$-absorber layer

To further examine defect-induced performance losses, a fixed bulk defect density of $10^{12}$ $cm^{-3}$ was combined with interface defect densities of $10^{15}$ $cm^{-2}$ at both the HTL/absorber and absorber/ETL junctions. Under this condition, $V_{oc}$ decreased to 0.9081 V and $J_{sc}$ to 41.316 mA/cm², while the fill factor increased to 87.28%, yielding a PCE of 32.75%. This indicates that even at low bulk defect densities, interface defects can significantly impact device output, underscoring the importance of interface engineering alongside bulk defect control.

### 4.5 TEMPERATURE ANALYSIS

The effect of operating temperature on the performance of the $AgCdF_3$-based solar cell was evaluated in the range of 300 K to 400 K. As the temperature increased, $V_{oc}$ decreased from 0.9081 V at 300 K to 0.7857 V at 400 K due to enhanced intrinsic carrier concentration and increased carrier recombination rates, which reduced the quasi-Fermi level separation. $J_{sc}$ remained nearly constant at around 41.31 mA/cm² over the entire temperature range, indicating minimal influence of temperature on photogeneration. However, the fill factor declined from 87.28% to 82.44%, leading to a drop in PCE from 32.75% to 26.75%. These results highlight the adverse impact of elevated temperatures on cell efficiency, emphasizing the need for effective thermal management strategies in practical applications.

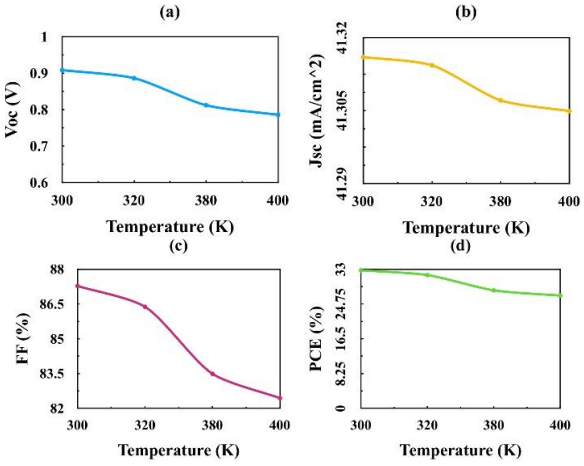


Fig. 6**:** $V_{oc}$(a), $J_{sc}$(b), FF(c), and efficiency(d) as a function of $AgCdF_3$-absorber-based solar cell.

## 5. Conclusion

$AgCdF_3$ is demonstrated as a lead-free, thermally robust, and high-efficiency perovskite absorber. SCAPS-1D simulations reveal that optimized NiO HTL, $ZrS_2$ ETL, absorber thickness, and interface engineering collectively minimize recombination and enhance charge extraction. The cubic structure and favorable band alignment underpin its exceptional stability and photovoltaic performance. While the reported efficiency represents an idealized upper limit under low-defect and lossless simulation conditions (bulk defect density of $10^{12}$ $cm^{-3}$ and interface defect densities of $10^{15}$ $cm^{-2}$), real-world factors such as grain boundary effects, optical losses, and non-radiative recombination could lead to lower experimental values. Nevertheless, these findings establish $AgCdF_3$ as a strong candidate for stable, high-performance, and environmentally sustainable photovoltaic applications, warranting further experimental exploration.

## References


[1] Ye, T., Wang, K., Hou, Y., Yang, D., Smith, N., Magill, B., Yoon, J., Mudiyanselage, R.R.H.H., Khodaparast, G.A., Wang, K. and Priya, S., 2021. Ambient-air-stable lead-free $CsSnI_3$ solar cells with greater than 7.5% efficiency. *Journal of the American Chemical Society*, 143, pp.4319–4328.

[2] Stranks, S.D. and Snaith, H.J., 2015. Metal-halide perovskites for photovoltaic and light-emitting devices. *Nature Nanotechnology*, 10, pp.391–402.

[3] Izam, N.S.M.N., Itam, Z., Sing, W.L. and Syamsir, A., 2022. Sustainable development perspectives of solar energy technologies with focus on solar photovoltaic — a review. *Energies*, 15, pp.1–15.

[4] Kojima, A., Teshima, K., Shirai, Y. and Miyasaka, T., 2009. Organometal halide perovskites as visible-light sensitizers for photovoltaic cells. *Journal of the American Chemical Society*, 131(17), pp.6050–6051.

[5] Jung, H.S. and Park, N.G., 2015. Perovskite solar cells: from materials to devices. *Small*, 11, pp.10–25.

[6] Green, M.A., Ho-Baillie, A. and Snaith, H.J., 2014. The emergence of perovskite solar cells. *Nature Photonics*, 8, pp.506–514.

[7] Miyasaka, T., Kulkarni, A., Kim, G.M., Öz, S. and Jena, A.K., 2020. Perovskite solar cells: can we go organic-free, lead-free, and dopant-free? *Advanced Energy Materials*, 10, pp.1–20.

[8] Orsch, G.H. and Paus, H.J., 1986. A new color center laser based on lead-doped $KMgF_3$. *Optics Communications*, 60, pp.69–73.

[9] Zhang, Y., Cleary, M., Wang, X., Kempf, N., Schoensee, L., Yang, J., Joshi, G. and Meda, L., 2015. High-temperature and high-power-density nanostructured thermoelectric generator for automotive waste heat recovery. *Energy Conversion and Management*, 105, pp.946–950.

[10] Snyder, G.J. and Toberer, E.S., 2008. Complex thermoelectric materials. *Nature Materials*, 7.

[11] Liu, E., Negm, A. and Howlader, M., 2021. Thermoelectric generation via tellurene for wearable applications: recent advances, research challenges, and future perspectives. *Materials Today Energy*, 20, p.100625.

[12] Zhang, F., Mao, Y., Park, T.J. and Wong, S.S., 2008. Green synthesis and property characterization of single-crystalline perovskite fluoride nanorods. *Advanced Functional Materials*, 18, pp.103–112.

[13] Pu, W., Xiao, W., Wang, J., Li, X. and Wang, L., 2021. Screening of perovskite materials for solar cell applications by first-principles calculations. *Materials & Design*, 198, p.109387.

[14] Zahra, F.T., Islam, M.M., Hasan, M.M., Islam, M.R. and Ahmad, S., 2024. DFT insights into the pressure-induced ultraviolet to visible band gap engineering of $TlMgF_3$ cubic halide perovskites for optoelectronic applications. *Journal of Physics and Chemistry of Solids*, 191, p.112037.

[15] Hossain, M.T., Hasan, M.M., Zahra, F.-T., Swargo, S., Dhroobo, R.A., Al Amin, M.R., Sieam, F.M.A., Disha, S.T. and Islam, M.R., 2024. A comprehensive DFT investigation of inorganic halide perovskites $GaXCl_3$ (X = Ca, Sr, and Ba) for optoelectronics application. *Physica B: Condensed Matter*, (2024), p.416131.

[16] Ravi, V.K., Yu, S.H., Rajput, P.K., Nayak, C., Bhattacharyya, D., Chung, D.S. and Nag, A., 2021. Colloidal $BaZrS_3$ chalcogenide perovskite nanocrystals for thin-film device fabrication. *Nanoscale*, 13(3), pp.1616–1623.

[17] Zahra, F.-T., Hasan, M.M., Hossen, M.B. and Islam, M.R., 2024. Deep insights into the optoelectronic properties of $AgCdF_3$-based perovskite solar cell using the combination of DFT and SCAPS-1D simulation. *Heliyon*, 10, p.e33096.

[18] Chabri, I., Benhouria, Y., Oubelkacem, A., Kaiba, A., Essaoudi, I. and Ainane, A., 2023. Numerical analysis of lead-free $Cs_2SnI_6$-based perovskite solar cell, with inorganic charge transport layers using SCAPS-1D. *Journal of Electronic Materials*, 52(4), pp.2722–2736.

[19] Mercy, E.N.V., Srinivasan, D. and Marasamy, L., 2024. Emerging $BaZrS_3$ and $Ba(Zr,Ti)S_3$ chalcogenide perovskite solar cells: a numerical approach toward device engineering and unlocking efficiency. *ACS Omega*, 9, pp.4359–4376.